

# Advanced LIVA/TIVA Techniques

R. Aaron Falk

OptoMetrix, Inc., Renton, Washington

## Abstract

LIVA (Light Induced Voltage Alterations) and TIVA (Thermally Induced Voltage Alterations) have demonstrated significant capability for fault isolation. A difficulty with both techniques is their use of a constant current source, whereas integrated circuits operate with a constant voltage source. A new technique that utilizes the constant current sensing of LIVA/TIVA, while allowing for use of constant voltage bias on the integrated circuit, has been developed. As a bonus, the technique is also significantly more sensitive (at least one order of magnitude) than the standard LIVA/TIVA approach.

## Introduction

A class of failure analysis techniques has evolved over the last several years, which utilizes a scanning laser beam\* to activate electrical characteristics of the test device. OBIC (Optical Beam Induced Current) [1] was the first of the class. It was later followed by LIVA [2], TIVA, and SEI (Seebeck Effect Imaging) [3-4]. The utilization of these laser probe techniques for failure analysis is primarily in fault isolation. TIVA, for example locates ohmic shorts due to the large resistance change with thermal heating that occurs at most shorts. SEI locates opens due to the electrical imbalance of the thermal electric effects at the open site. A significant feature of these techniques is their ability to work from both the topside and backside. Backside analysis is critical for "flip-chip" packages and devices with multiple metal layers, which obscure visibility from the topside.

One difficulty with most of these fault isolation techniques is the need for constant current biasing of the device. Nearly all integrated circuits require constant voltage source for correct operation. Another issue is noise level, which can obscure weak signals. A new technique has been developed, which allows for constant current biasing of the circuit, while still allowing for constant current signal sensing. A further advantage of the technique is its ability to reject many noise sources.

Reduced noise means reduced image acquisition times and higher quality images. Higher quality

allows for extraction of image detail, which can potentially lead to identification of the specific fault.

## Advanced LIVA/TIVA - XIVA

### General Approach

A basic system for performing these fault isolation techniques utilizes a laser scanning (confocal) microscope to sequentially scan a focused laser spot over the integrated circuit. Scanning can be performed from the front or backside through selection of the laser wavelength. Some device preparation for backside scanning is also necessary [5-6]. In addition to unzipping the package, thinning and polishing of the substrate is generally required. Use of an anti-reflection coating improves image quality and allows more of the laser beam to penetrate into the substrate.

As the focussed laser beam passes over an integrated circuit, it causes changes in the device electrical characteristics through two effects, generation of photocarriers and heating. If the laser wavelength is chosen to be below the semiconductor bandgap<sup>†</sup>, then only heating occurs. Shorter wavelengths, above the bandgap, will produce both photocarriers and heating. However, photocarrier effects are orders of magnitude stronger and generally dominate any thermal signals. Both photocarrier generation and heating can cause changes in the circuit resistance (photoconductive and thermal-conductive effects) and cause currents to flow (photovoltaic and Seebeck or thermal couple effects).

For the photovoltaic and Seebeck effects, no external bias is needed to observe a signal. For the photoconductive and thermal conductive effects, application of a constant current to the integrated circuit causes small voltage alterations to occur across the device in response to the optically induced changes in the circuit resistance.

The main application of these techniques, to date, has been fault isolation. In some cases, faults are located by comparison of an image from a "good" sample to the image of a failed device. Comparison is not

---

\* Scanned electron or ion beams can also be used for activation in some cases.

---

<sup>†</sup> For topside probing, a dark coating can be used to allow surface heating without photocarrier generation.

<b><i>Technique</i></b>	<b><i>Physics</i></b>	<b><i>FA Applications</i></b>
<b>OBIC (Optical Beam Induced Current)</b>	Photovoltaic Effect	Location of Junction Defects
<b>LIVA (Light Induced Voltage Alterations)</b>	Photoconductive Effect	Location of Open Junctions and Substrate Damage
<b>SEI (Seebeck Effect Imaging)</b>	Seebeck (Thermal-Voltaic/Thermal Couple) Effect	Location of Opens
<b>TIVA (Thermally Induced Voltage Alterations)</b>	Thermal-Conductive Effect	Location of Shorts, Vias with Incorrect Resistance

Figure 1 Different measurement techniques that can be performed with the XIVA system.

generally required for TIVA and SEI, which only produce signals at the fault, associated drivers and drive lines.

The types of faults detected are determined by the detailed physics of the laser interaction. The table in Figure 1 summarizes the capabilities of each technique.

### Sensing Techniques

The original LIVA and TIVA approach utilized a constant-current source bias on the test device. A change in the test device impedance results in a change in the voltage across the device. This change is then amplified by an AC coupled amplifier, which rejects the DC voltage on the device.

The alternative to TIVA is exemplified by OBIRCH (Optical Beam Induced Resistance Change) [7], which utilizes a constant voltage bias and places a current sensor in series with the test device. This approach is more compatible with how integrated circuits are normally biased. However, experimental results have shown that TIVA can be orders of magnitude more sensitive than OBIRCH [3].

Our new approach, which we have designated XIVA\* (Externally Induced Voltage Alterations), allows constant voltage biasing of the device, while maintaining the high sensitivity of constant current sensing. The simultaneous application of constant voltage bias to the test device coupled with constant current sensing appears, at first, to be contradictory functions. The contradiction is resolved by realizing that the voltage bias is a low frequency "signal" and

the constant current sensing is a high frequency signal. The bias is a constant, whereas, the XIVA signal only occurs while the scanning laser passes over the failure sight. An ideal current choke, placed in the bias lines, produces the desired functional separation (see Figure 2). At low frequencies, the current choke has no effect on the circuit and proper voltage bias can be established. However, when the scanning laser causes a sudden change in impedance of the test device, the current choke acts to temporarily suppress any changes in the DC current level. Constant current sensing with constant voltage biasing is thereby achieved.

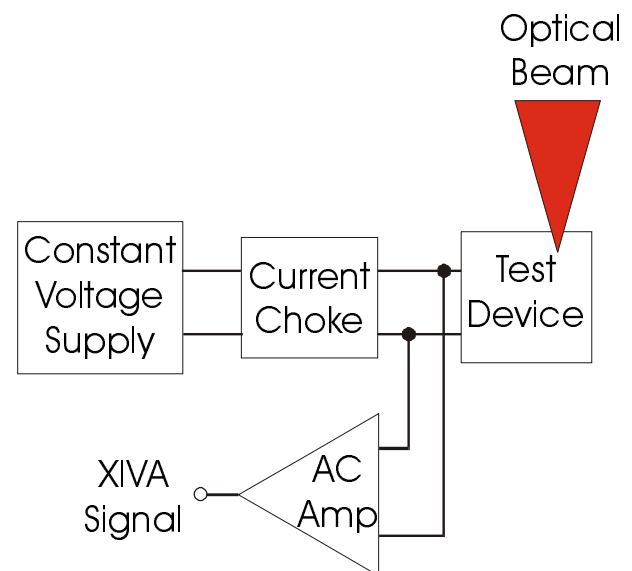


Figure 2 Block diagram of XIVA head utilizing current choke to separate bias and sensing functions.

\* Patent Pending

Practical realization of the XIVA circuit can be obtained by several means. The simplest approach is the use of a pair of high-inductance choke coils placed in the voltage bias lines.

### Noise Issues

The time it takes to acquire an image of a failure with a clear signal is proportional to the square of the system noise. Clearly, decreased noise levels produce great benefit in image acquisition time. The ability to pull out fine detail in the image is an additional benefit of decreased noise.

Noise can occur from a variety of sources:

- Preamplifier
- Test Device
- Environment
- Power Supply

Preamplifier noise represents a fundamental limit. This limit can be brought down into the microvolt range for typical bandwidths needed for image acquisition. At these low voltage levels, other noise sources become rather important.

The test device will produce Johnson noise. This noise is only an issue at fairly high resistance levels, on the order of 100,000 ohms or higher. However, test devices are not pure resistors. They contain active transistors, protection diodes, etc., which can add significantly to the noise levels. Maintaining the device in a static condition during image acquisition is also critical.

External pickup can be a major noise problem. Test devices are typically mounted into a PC board for supplying power and I/O connections. These boards are rarely laid out with noise pickup in mind. Pickup noise due to board layout has been shown experimentally to increase noise levels by as much as a factor of 15, even in a relatively benign noise environment. Shielding can help with pickup noise. However, the pickup is often magnetic, which is very difficult to shield against. PC board designs should utilize short connections and avoid large loops in lines, to obtain optimum performance. An example of noise pickup for bad and good board design is shown in Figure 3. The current dependency of the noise relates to the effective impedance of the test device, which for non-linear devices is current (voltage) dependent.

Power supplies are also a potential noise source at the microvolt level. Only top quality supplies come close to meeting these requirements.

The XIVA approach has demonstrated factors of 10-20 improvement in SNR over the standard constant current approach. The improvement results primarily from XIVA's ability to reject a number of these noise sources. The circuit is clearly balanced with the signal passing through a differential preamplifier. A high degree of common noise rejection is achieved with this technique. A serendipitous aspect of the circuit is that the current choke doubles as a filter for the power supply noise at high frequencies. The AC coupled preamplifier filters out any remaining low-frequency power supply noise.

## Results

### Signal Characteristics

Generally, OBIC and LIVA signals are quite large compared to noise. TIVA and SEI signals can be quite weak, especially from the backside. Additionally, signal reduction occurs at low magnification, where the laser spot size is large and less efficient at heating the device structure. Resistance changes in TIVA can be only a few parts in  $10^5$  for a level 5 short at low magnification, for example.

A standard test structure was utilized to compare the XIVA technique to TIVA. The structure consists of metal serpentines with an insulating layer between the metal and the substrate. The serpentine structure is a simple high-resistance path with low resistance connections. Figure 4 shows two images of a series pair of serpentines at low magnification (2.5X\* and numerical aperture of 0.06). The first image is a backside TIVA image and the second image is a backside thermal XIVA image. Laser power was identical for both images (~ 50 mW at 1340 nanometers from the objective aperture). The AC coupled preamplifier and acquisition times were also identical for both images. The only difference was the use of a constant current source for the TIVA image and a constant voltage source with a current choke for the XIVA image. In fact, the constant current source utilized the same input voltage reference as the constant voltage source. The difference in signal-to-noise ratio is readily apparent.

A real world example is shown in Figure 5. The sample is an SRAM with a level 3 short. The first thermal XIVA image was obtained at 2.5X, in order to localize the fault location. Image acquisition time was less than 1 second. At 10X magnification, the rather large spot in the previous image is resolved into three distinct spots. Significant detail is seen in

---

\* 2.5X corresponds to a field-of-view of ~ 5 millimeter. Field-of-view at other magnifications scales linearly.

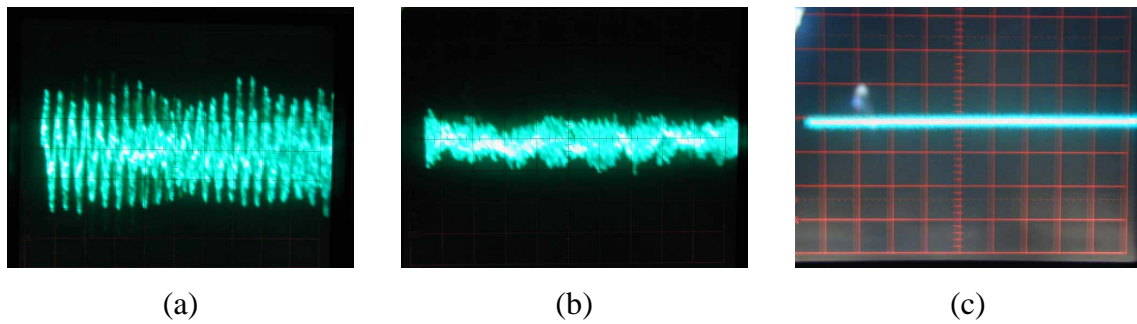


Figure 3 Photos of scope traces showing relative noise pickup on poorly laid out circuit board. All traces are at the same volts/division. (a) Noise pickup at low current,  $\sim 0.3$  mA. (b) Noise pickup at higher currents  $> 1.0$  mA. (c) System noise limit with good circuit board layout and use of twisted pair leads.

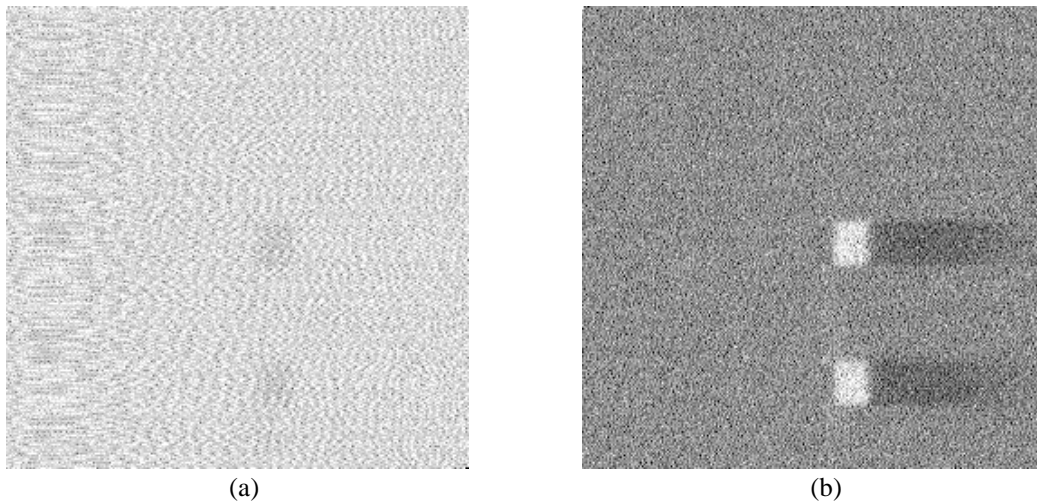


Figure 4 Comparison of signals from backside TIVA (a) and thermal XIVA (b) for metal serpentine test structures. The improved signal-to-noise performance of XIVA is clear. Dark versus light signals relate to sign change for XIVA sensing.

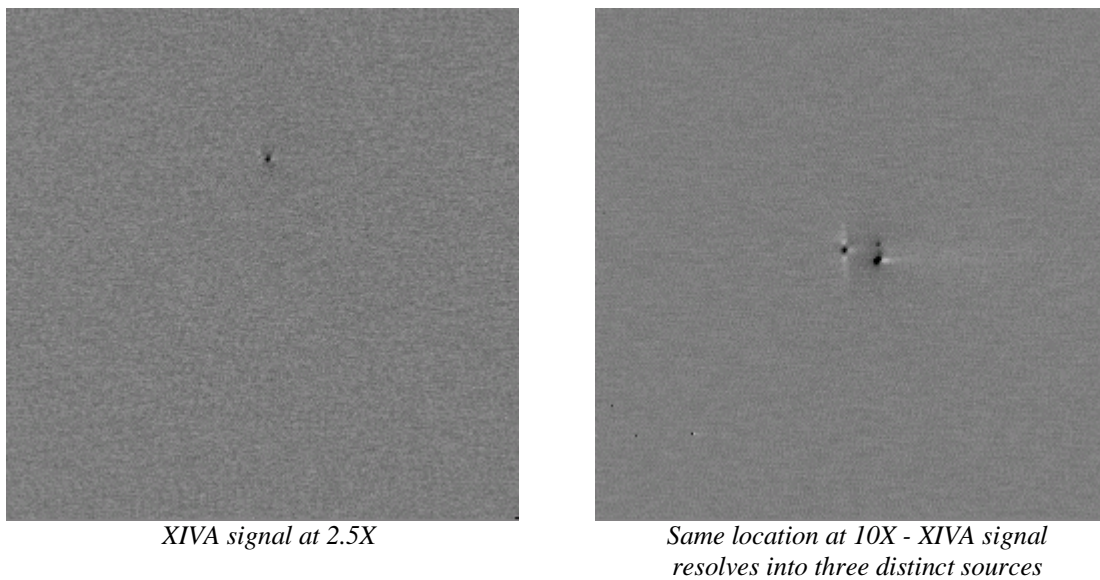


Figure 5 Thermal conductive and thermal electric XIVA signals of level 3 short in SRAM. Image (a) is at 2.5X and image (b) is at 10X. Image (b) resolves the low resolution image (a) into three distinct sources. Scan time is  $\sim 1$  second with laser power of  $\sim 50$  mW at 1340 nm from objective.

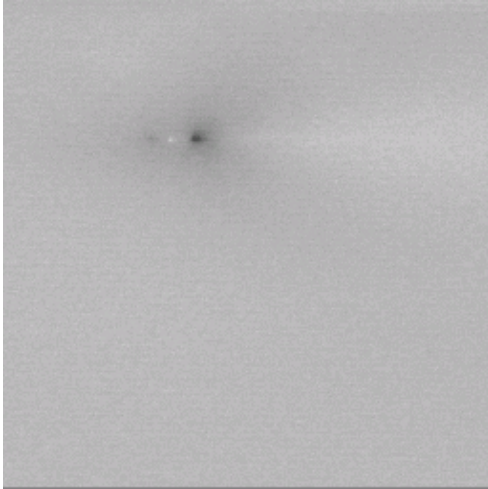


Figure 6 Thermal XIVA image of level 5 short in SRAM at 20X.

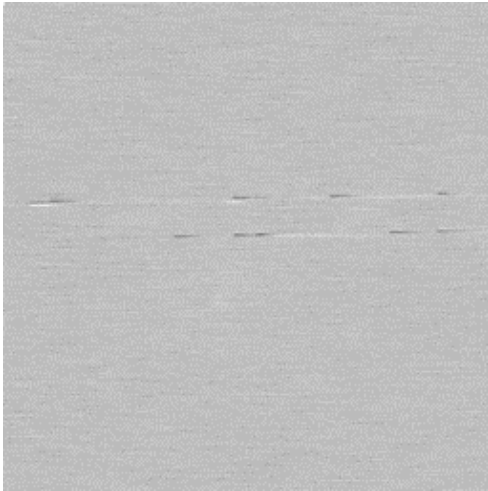


Figure 7 Expanded image of SRAM in Figure 6 at 2.5X and higher current level showing FET turn on.

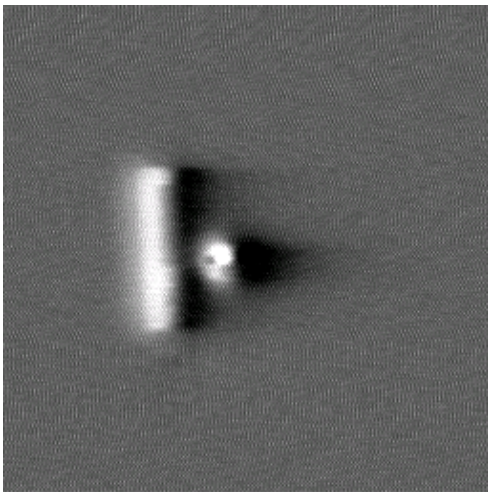


Figure 8 Thermal XIVA image of drive FET at 10X.

each spot, e.g. vertical white structure in the leftmost spot and white "tails" in two of the spots. The 2.5X TIVA signal was barely observable for a 1 second acquisition time with this sample.

Thermal XIVA images of a level 5 short in an SRAM are shown in Figures 6 and 7. Level 5 shorts can be very difficult to find from the backside due to the heat diffusion in the intervening metal layers. The signal shown in Figure 6 was due to a thermal resistance change of only a few parts in  $10^5$ .

## Diagnostic Potential

To date, the primary use of OBIC, LIVA, TIVA, and SEI has been fault isolation. The availability of high quality imagery opens the door for more detailed diagnostic techniques. The three separate signals (spots) seen in the XIVA thermal image in Figure 5b are clearly different. The left most signal shows a vertical white structure around a black dot. A white "tail" can be seen to the right of the black dot. The signal to the upper right of the group is a single black dot. The lower right dot is a bit larger and has a white tail.

The physical interaction of the laser activation and circuit response is clearly different in each of these three signals. The vertical white-black-white structure, for example, is characteristic of a Seebeck effect. Further evidence for Seebeck effect is the existence of the signal at zero voltage bias. The tail structure is demonstrably an effect of the device physics as well, since one of the three signals shows no tail.

The tails relate directly to the recovery time of the fault. A simple model of the device temporal response is given by

$$\partial\rho/\partial t = G - \rho/\tau \quad (1)$$

where  $\rho$  is the device response,  $G$  is a generation term due to the laser illumination, and  $\tau$  is a recovery time. In the case of photoconductive effects,  $\rho$  would be the carrier density generated by the laser illumination,  $G$ , and  $\tau$  would be the carrier recombination time. For thermal effects,  $\rho$  is the temperature and  $\tau$  is the thermal recovery time. In both cases the change in device electrical parameters, e.g. resistance, is assumed to be linearly related to  $\rho$ .

The effect of the AC coupled amplifier in the sensing circuit is to produce the derivative of the device response. The electronics, which includes the

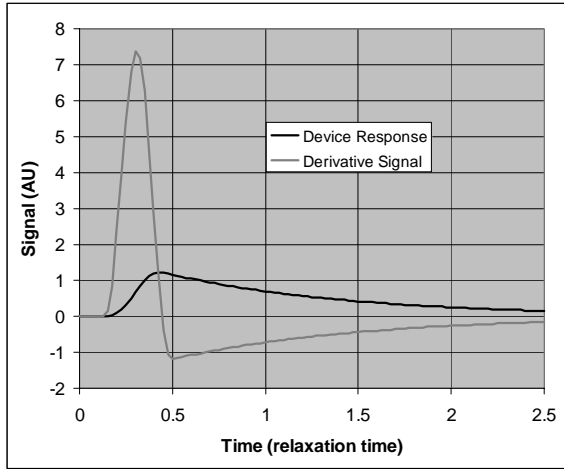


Figure 9 Model of XIVA signal response.

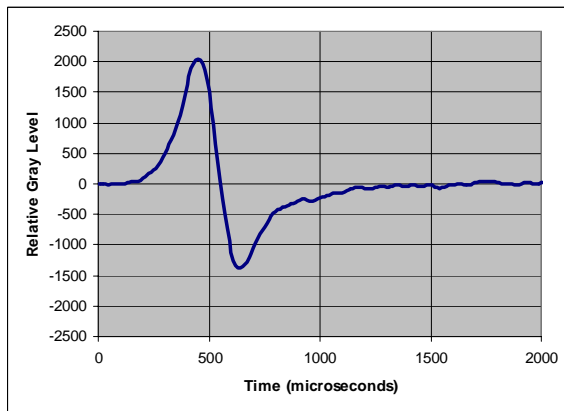


Figure 10 Graph of thermal XIVA signal versus time for FET in Figure 8.

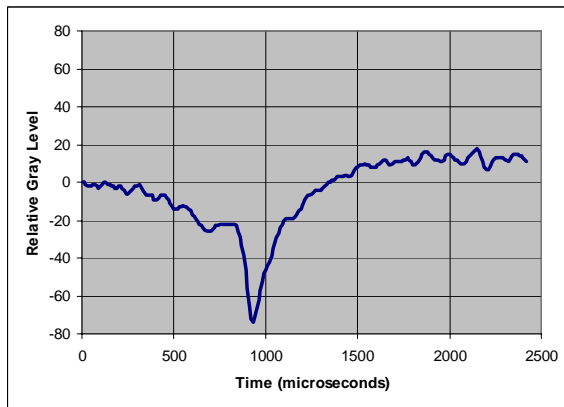


Figure 11 Graph of signal versus time for level 5 short in Figure 6. Note sign shift compared to FET signal.

reactance of the test device will also limit the high end frequency response of the signal. Figure 9 shows a numerical solution to Equation 1 for square pulse illumination coupled with a high frequency rolloff term.

The XIVA images shown in this paper all derive from a left-to-right raster scan with a pixel dwell time of  $\sim 10$  microseconds. Thus, left-to-right position in the images also represents a time response for an isolated signal. A plot of the response of a portion of the FET signal (Figure 8) is shown in Figure 10. The similarity to Figure 9 is quite clear. The tail indicates a cooling time of the FET of  $\sim 100$   $\mu$ Sec. Figure 11 shows the time response of the level 5 short in Figure 6. Note that the short signal is of the opposite sign as the FET signal. The thermal recovery time of the short is sufficiently long ( $> 1000$   $\mu$ Sec) that it is difficult to estimate. The FET, located within the substrate, is clearly cooling off much faster than the level 5 short, located deep within highly thermally insulating dielectric material. The potential for estimating the depth of a defect from the thermal recovery time is clear. Determining the accuracy of such estimates will require further study. Detailed thermal modeling of the surrounding geometry will clearly aid in producing accurate results.

Information on the failure is also available in its response with laser intensity and current. Cole, et al. have described the effect of signal response versus laser intensity [4]. Figure 12 shows a plot of the signal response versus current for a manufactured, metal-to-metal FIB short. A linear signal response with current would be expected from this simple ohmic short. Surprisingly, the signal saturates at fairly low current levels.

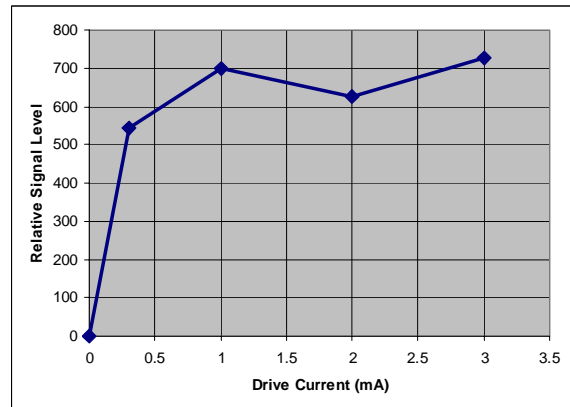


Figure 12 Signal versus drive current for level 5 short in Figure 6.

Figure 7 shows the reasons behind this non-linear current response. The device bias voltage is increasing as the current level increases, which causes the active elements in the device to “turn on” and pull current (voltage) away from the actual failure. Clearly, information on the nature of the circuit failure is contained within the XIVA thermal signal response versus bias. For complex circuits, this information may prove difficult to decipher, however.

Photovoltaic (OBIC) and photoconductive (LIVA) failures were not available for XIVA testing at the time of this writing. However, the appearance of recovery times relating to carrier recombination and sweep out can be expected. Signal versus bias level can also be measured. Effort is needed to determine the potential value of these measurements.

## Summary and Conclusions

An advanced technique for failure localization has been demonstrated. This XIVA technique allows constant voltage device biasing, while utilizing constant current signal sensing. The XIVA technique allows photovoltaic (OBIC), photoconductive (LIVA), thermal electric (SEI) and thermal conductive (TIVA) measurements through the power lines or signal lines with the test device operating under correct, voltage bias conditions.

An additional, feature of the XIVA technique is strong rejection of external noise sources. Order of magnitude noise improvements have been observed. Decreased noise produces decreased image acquisition times, along with improvements in image quality.

Although it is too early to produce definitive statements, the potential to utilize XIVA for failure diagnosis seems apparent. Further effort to correlate signal appearance, laser power response, and voltage/current response to specific failure types is needed.

## Acknowledgements

The author would like to thank Ed Cole of Sandia National Laboratories for discussions on the interpretation of several of the images. Thanks also go to Ted Levin and Dave Vallett of IBM and Edward Budiarto of Intel for supplying test samples.

## References

1. Tony Wilson "Theory and Practice of Scanning Optical Microscopy", Academic Press, London (1984)
2. E.I. Cole, Jr., J.M. Soden, J.L. Rife, D.L. Barton, and C.L. Henderson, "Novel Failure Analysis Techniques Using Photon Probing with a Scanning Optical Microscope", IRPS, 388-98 (1994).
3. E.I. Cole, Jr., P. Tangyonyong, and D.L. Barton, "Backside Localization of Open and Shorted IC Interconnections", IRPS, 129-136 (1998).
4. E.I. Cole, Jr., P. Tangyonyong, D.A. Benson and D.L. Barton, TIVA and SEI Developments for Enhanced Front and Backside Interconnection Failure Analysis", ESREF (1999).
5. B.V. Davis, "Antireflection Coatings for Semiconductor Failure Analysis", ISTFA, 155-60. (2000).
6. P. Perdu, R. Desplats, and F. Beaudin, "Comparative Study of Sample Preparation Techniques for Backside Analysis", ISTFA, 161-72 (2000).
7. K. Nikawa and S. Inoue, "Various Contrasts Identifiable from the Backside of a Chip by 1.3 um Laser", ISTFA 387-392 (1996).